Geophysical Research Letters

RESEARCH LETTER
10.1029/2019GL082228

Large Eddies Regulate Turbulent Flux Gradients in Coupled Stable Boundary Layers

Changxing Lan[1], Heping Liu[1], Gabriel G. Katul[2,3], Dan Li[4], and Dennis Finn[5]

[1]Laboratory for Atmospheric Research, Department of Civil and Environmental Engineering, Washington State University, Pullman, WA, USA, [2]Nicholas School of the Environment, Duke University, Durham, NC, USA, [3]Department of Civil and Environmental Engineering, Duke University, Durham, NC, USA, [4]Department of Earth and Environment, Boston University, Boston, MA, USA, [5]NOAA, Air Resources Laboratory, Idaho Falls, ID, USA

Abstract Due to strong mean wind shear, the stable boundary layer (SBL) becomes vertically coupled. In a coupled SBL, large turbulent eddies enhance cross-layer mixing and vertically mix turbulent kinetic energy. However, large gradients in momentum and heat fluxes are frequently observed, degrading the performance of Monin-Obukhov similarity theory. It is shown that increased vertical gradients of mean variables (i.e., wind speed and potential temperature) can cause flux gradients. This process is operated upon by downward penetrating large eddies with altered phase difference, contributing unevenly to fluxes and thus causing flux gradients. In the coupled SBL with small gradients in mean variables, large eddies are vertically synchronized, contributing evenly to fluxes across layers and thus causing small flux gradients. As turbulent production becomes weak and the cross-layer difference in turbulent flux transport increases, large eddies become less vertically synchronized, contributing unevenly to fluxes across layers and thus causing large flux gradients.

Key Points:
- Vertical gradients of turbulent fluxes and turbulent kinetic energy (TKE) in the stable boundary layer (SBL) are experimentally analyzed
- Cross-layer phase difference of large eddies is indicative of momentum and heat flux gradients even when TKE gradients are small in the SBL
- Weak turbulent production and different cross-layer turbulent flux transport associated with large eddies lead to large flux gradients

Supporting Information:
- Supporting Information S1

Correspondence to:
H. Liu,
heping.liu@wsu.edu

Citation:
Lan, C., Liu, H., Katul, G. G., Li, D., & Finn, D. (2019). Large eddies regulate turbulent flux gradients in coupled stable boundary layers. *Geophysical Research Letters*, *46*. https://doi.org/10.1029/2019GL082228

Received 29 JAN 2019
Accepted 6 MAY 2019
Accepted article online 9 MAY 2019

1. Introduction

Significant efforts have been made to inquire about the vertical structure of the nocturnal stable boundary layer (SBL), the energetics of turbulent eddies, and flux exchanges above uniform surfaces given their relevance to improving weather and climate models (Acevedo et al., 2016; Mahrt, 2014; Sun et al., 2012). These models rely on Monin-Obukhov similarity theory (MOST) derived for stratified stationary flows above planar homogeneous surfaces in the absence of subsidence and mean pressure gradient at high Reynolds numbers (Monin & Obukhov, 1954). Applying these MOST assumptions to the mean momentum and mean potential temperature budgets leads to momentum and kinematic sensible heat fluxes being constant with height above the ground (Dyer & Hicks, 1970). The applicability of the constant-flux assumption in the SBL is often associated with the so-called SBL coupling states. In the weakly stratified SBL with strong vertical mixing, the turbulence Dougherty-Ozmidov length scale is much larger than the measurement height, and MOST appears to be applicable (Katul et al., 2014; Monahan et al., 2015). However, strongly stratified SBL is characterized by intermittent turbulence, weaker vertical mixing, and frequent intrusions of submeso motions (Mortarini et al., 2018; Sorbjan & Czerwinska, 2013). In this regime, the layers within the SBL are weakly coupled and there is a broad recognition that MOST does not capture the flow statistics. Amendments to MOST in such regime remain the subject of active research and are the focus here.

The relation between turbulent kinetic energy (TKE) profiles and near-surface wind speed has been proposed to characterize the coupling state of the SBL (Liang et al., 2014; Sun et al., 2012). Under low mean wind speed conditions, turbulence is largely suppressed by thermal stratification in the vertical direction and turbulent eddies are confined to thin layers. These eddies are presumed to be detached from the ground (i.e., z-less scaling), leading to a vertically layered as well as decoupled SBL. Under such conditions, the flow statistics within the SBL are poorly correlated across layers, and considerable vertical gradients in TKE and turbulent fluxes are observed (Lan et al., 2018).

As the near-surface mean wind speed exceeds a site-specific threshold, the sign of the vertical gradient of TKE abruptly switches and the SBL becomes coupled (Acevedo et al., 2016; Lan et al., 2018). In such a coupled SBL, the enhanced mechanical mixing allows large eddies with large vertical scales to develop. Such eddies cause effective transport of warm air from aloft to be brought downward and cold air near the ground to be brought upward, leading to enhanced sensible heat flux to the surface (Lan et al., 2018).

An increase in the downward sensible heat flux then increase the buoyant destruction of TKE countering its mechanical generation. The downward sensible heat flux is primarily determined by the small cross-layer temperature difference and the large turbulent heat diffusivity associated with large eddies (Acevedo et al., 2016; Sun et al., 2016). These large eddies also enhance cross-layer correlation among turbulent flow variables leading to relatively small cross-layer differences in TKE and velocity variances (Lan et al., 2018; Mahrt et al., 2018). It is generally argued that MOST is applicable in such a coupled SBL. However, large vertical variations in momentum and heat fluxes (i.e., flux divergence or convergence; hereafter flux gradients) remain frequently observed in the coupled SBL, invalidating the applicability of MOST. For instance, momentum and heat fluxes increase with height due to elevated shear-generated turbulence (Mahrt et al., 2018). Burst of momentum and heat fluxes caused by intermittent turbulence also lead to unequal fluxes between layers (Jensen et al., 2016). It remains unclear as to what role large eddies play in regulating the vertical gradients of momentum and kinematic heat fluxes even in a reasonable coupled SBL, which is the main compass of the work.

Data collected by four eddy covariance (EC) systems situated on a 62-m tower are analyzed, aiming to address (i) the cross-layer differences in momentum and kinematic heat fluxes in a coupled SBL (as defined by the vertical gradient of TKE), (ii) the linkage between flux gradients and the background profiles of mean wind speed and potential temperature, and (iii) the roles of large eddies in regulating flux gradients in a coupled SBL. Theoretical arguments are then made to support the experimentally documented features, demonstrating how large eddies are linked to turbulent flux gradients under varying turbulent production regimes. The results reported here demonstrate that the background vertical profiles of mean wind speed and potential temperature cause flux gradients in the coupled SBL. This process is operated upon by large eddies that penetrate downward across layers, as indicated by the relation between cross-layer phase difference of large eddies and flux gradients.

2. Experiment, Data, and Methodologies

2.1. Experimental Site, Instrumentation, and Post Field Data Processing

EC data were collected over a flat terrain at the Idaho National Laboratory site, southeast Idaho (43.59 °N, 112.94 °W; 1,500-m above mean sea level; Figure S1 in the supporting information). The four EC systems were mounted at 2, 8, 16, and 60 m on the tower and each of them consisted of a 3-D sonic anemometer (CSAT3, Campbell Scientific, Inc.) and an infrared CO_2/H_2O gas analyzer (IRGA, LI7500A, LiCor Inc.). Sonic anemometers measured the three-dimensional wind components (u, v, and w that denote longitudinal, lateral, and vertical velocities, respectively). The sonic derived air temperature (T) was also used to determine temperature statistics (i.e., potential temperature, θ) and sensible heat fluxes. The IRGAs measured density of water vapor (ρ_v) and CO_2 (ρ_c) at high frequency. The measured time series acquired with four dataloggers (CR5000, Campbell Scientific, Inc.) from the sonic anemometers and IRGAs were sampled at 10 Hz and stored for postfield processing. The details about the site, general meteorological conditions during this field campaign, and other instrumentations have been presented in prior studies (Finn et al., 2015, 2016) and are not repeated here.

Detailed post field data processing procedures have been provided elsewhere (Lan et al., 2018; Liu et al., 2016). Briefly, these procedures include (1) removing spikes/noise from the raw 10-Hz time data and gap filling the time series with linear interpolation (Gao et al., 2016); (2) double rotation for the three-dimensional wind components (Kaimal & Finnigan, 1994); (3) calculation of averages, variances, and covariances using the unweighted block average method; (4) sonic temperature correction (Liu et al., 2001; Schotanus et al., 1983) and density correction (Webb et al., 1980); and (5) data quality check (Foken et al., 2005). To reduce "contamination" from submeso motions on turbulent fluxes, coordinate rotation and calculation of turbulent statistics are performed over unweighted 5-min intervals. These 5-min statistical quantities are then averaged to 30-min means to represent SBL states over a relatively long period (Lan et al., 2018). Therefore, a coupled SBL is defined by requiring the 30-min-averaged stability parameter ($\zeta_l = z/\Lambda$, where z is the observation height from the ground and Λ is the local Obukhov length) to range between 0 and 100 and the near-surface mean wind speed ($U_{2\mathrm{m}}$, where the subscript "2m" indicates that the measurement height is 2-m above the ground) to be larger than 4 m/s (the choice of 4 m s^{-1} will be further elaborated in

section 3). In the following sections, each 30-min run in the coupled SBL regime is divided into six 5-min runs (a total of 420 5-min runs).

2.2. Ensemble Empirical Mode Decomposition (EEMD) and Phase Difference

Due to the nonlinearity and nonstationary of turbulence time series in the SBL, EEMD, which is adaptive without requiring a priori assumptions and "extra" ad hoc postprocessing (Huang et al., 1998; Huang & Wu, 2008), is employed for our analysis. Specifically, it uses a sifting process to decompose a time series $x(t)$ into a finite number of intrinsic mode functions (IMF_i) as well as an overall residual ($r(t)$) given as

$$x(t) = \sum_{i=1}^{n} IMF_i(t) + r(t). \tag{1}$$

To reduce the influence of nonturbulent submeso motions, the EEMD is applied to 5-min time series of turbulent fluctuations (i.e., u', w', and θ'). For each 5-min run, nine amplitude-frequency modulated IMF_i (i.e., $n = 9$) are extracted with one overall residual r_{10} that still contributes to the total variance or covariance. Each oscillatory component (i.e., each IMF) has its mean frequency ($\overline{\omega}$) estimated as follows:

$$\overline{\omega}_i = \frac{\int_0^\infty f S_i(f) df}{\int_0^\infty S_i(f) df}, \tag{2}$$

where $S_i(f)$ is the Fourier spectrum of $\mathrm{IMF}_i(t)$ (Huang et al., 1998; Wei et al., 2017). Taking advantage of the additivity of the time domain IMF_i, the sum of certain oscillatory components can be interpreted as a signal for turbulent eddies with specific scales (Gao et al., 2017).

Statistically, the influence of turbulent eddies on covariances (i.e., vertical fluxes) depends on not only the magnitude of fluctuations (i.e., w' and θ' for heat flux) but also the phase difference between these two time series (Gao et al., 2017; Li & Bou-Zeid, 2011). The instantaneous phase difference between these two time series can be calculated based on Hilbert transform

$$\Phi(t) = \tan^{-1}\left(\frac{\mathrm{Im}[HCS^{xy}(t)]}{\mathrm{Re}[HCS^{xy}(t)]}\right), \tag{3}$$

where $HCS^{xy}(t)$ is Hilbert cross-spectrum. In the supporting information, how the phase difference between two time series influences flux gradients is described and the method used to calculate the Hilbert transform is introduced (Texts S1 and S2 and Figure S2).

3. Results and Discussion

3.1. Small Cross-Layer Differences in TKE But Large Flux Gradients in a Coupled SBL

The relation between TKE and $U_{2\mathrm{m}}$ is commonly used to categorize whether a SBL is decoupled or coupled (Acevedo et al., 2012, 2016; Lan et al., 2018). Using the same dataset, Lan et al. (2018) found that when $U_{2\mathrm{m}}$ is smaller than 4.0 m/*s*, the SBL at this site is vertically decoupled as reflected by the large cross-layer-differences in TKE and velocity variances shown in Figure S3. Conversely, when $U_{2\mathrm{m}}$ is larger than 4.0 m/s, the SBL becomes vertically coupled with small vertical gradients of TKE and velocity variances (Figure S3). The near-surface wind speed of 4.0 m/s is thus considered as the threshold for the transition between decoupled and coupled SBL states for this site. Moreover, the coupling depth was found to vary between 16 and 60 m (Lan et al., 2018). Therefore, data collected at 60 m are excluded from the analysis. Here the cross-layer difference is defined as

$$\Delta S = \left|\frac{S_{upper} - S_{lower}}{S_{lower}}\right| * 100\%, \tag{4}$$

where S denotes an arbitrary variables to be analyzed, including TKE, velocity variances (i.e., ${\sigma_u}^2$, ${\sigma_v}^2$, and ${\sigma_w}^2$), covariances (i.e., $\overline{u'w'}$, and $\overline{w'\theta'}$), and third-order turbulent flux transport (i.e., $\overline{w'u'w'}$ and $\overline{w'\theta'w'}$) for reasons to be described later. As shown in Figures S4 and S5 for coupled SBL states only (i.e., $U_{2\mathrm{m}} > 4.0$ m/s), a clear pattern of variations in turbulence statistics with $U_{2\mathrm{m}}$ is absent, indicating that the near-surface mean wind speed is not the predominant control describing the vertical profiles of TKE,

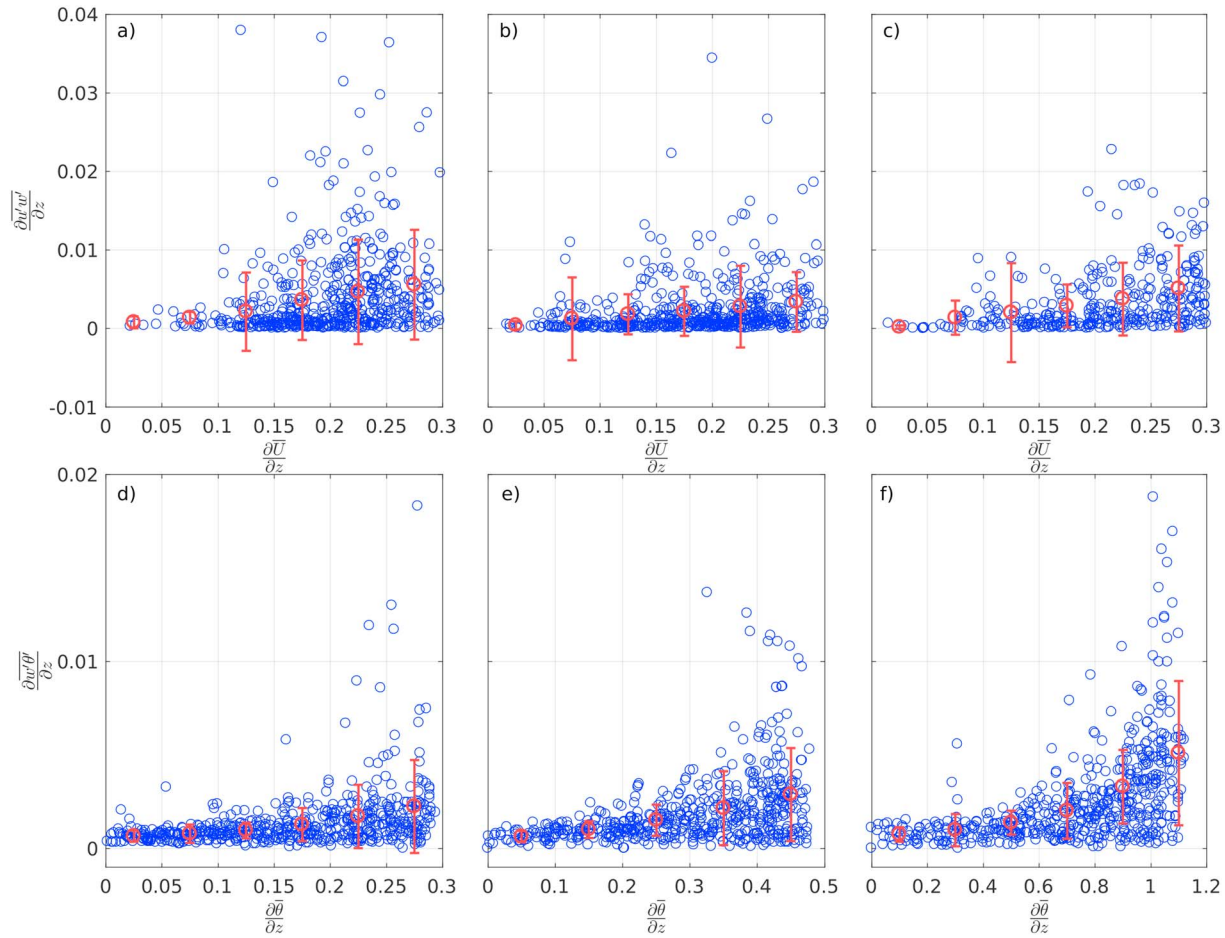

Figure 1. Variations of the gradients of momentum flux (m/s^2; a–c) and kinematic heat flux (K/s; d–f) with the vertical gradients of mean wind speed (m/s) and potential temperature (K/m), respectively. Panels from left to right correspond to the results between 16 and 8 m, between 8 and 2 m, and between 16 and 2 m, respectively. The red circles and error bars refer to the bin averages and corresponding standard deviations, respectively.

variances, and fluxes in the coupled SBL. As shown in Table S1, the relative differences in TKE and velocity variances are small, whereas the relative differences in momentum and kinematic heat fluxes are 3–5 times larger than their TKE and variances counterparts. In addition, the relative differences in third-order turbulent flux transport are unexpectedly large (i.e., at least one order larger than their flux counterparts). Clearly, these features demonstrate that even in the coupled SBL with comparable variances between layers, the gradients of momentum and heat fluxes can vary from small to substantially large. The large flux gradients indicate that MOST may not be applicable in the coupled SBL. What mechanisms cause such large gradients in momentum and kinematic heat fluxes in the coupled SBL? Under what conditions the flux gradients are small so that MOST is applicable in the coupled SBL? These questions motivate exploring the underlying causes for the flux gradients experimentally in the coupled SBL ($U_{2m} > 4.0$ m/s).

3.2. Large Eddies and Their Roles in Regulating Cross-Layer Turbulence and Flux Divergences or Convergence in a Coupled SBL

While near-surface mean wind speed does not explain the flux gradients in the coupled SBL, the flux gradients show dependence on the vertical gradients of mean wind speed and potential temperature (Figure 1). As shown in Figure 1, the flux gradients increase monotonically with the gradients of the two mean variables. In a previous study using the same data set, we found that in the coupled SBL, strong shear and weak stratification allow large eddies to develop, thereby leading to high cross-layer correlations among turbulent fluctuations and enhanced cross-layer momentum and heat transport (Lan et al., 2018). These results lead us to hypothesize that the increased vertical gradients of mean wind speed (potential temperatures) alter the

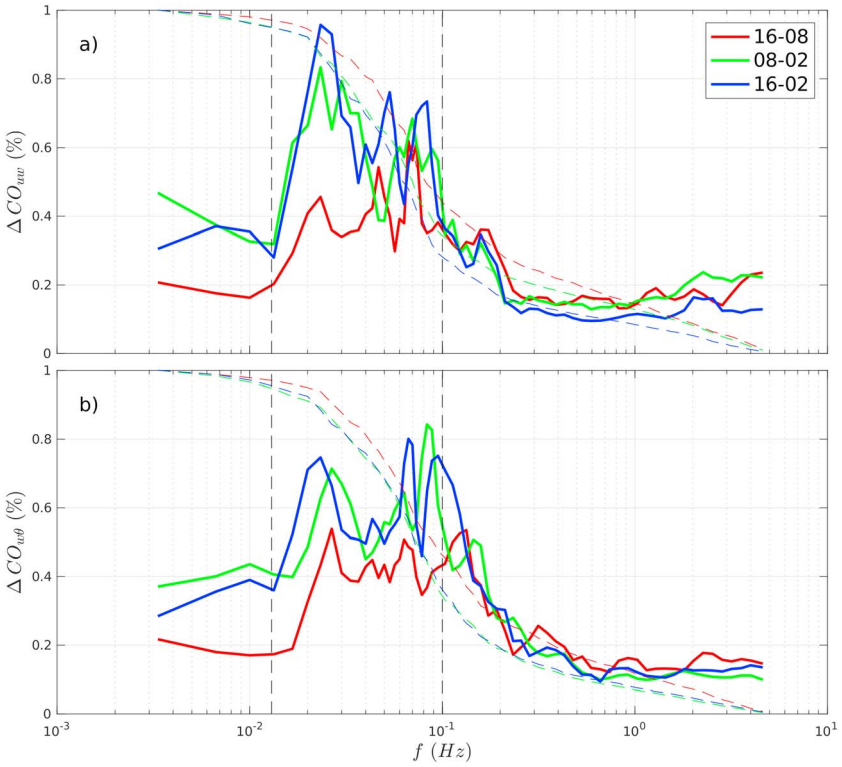

Figure 2. Cross-layer differences in momentum flux (a) and kinematic heat flux (b) as a function of the natural frequency. Red, green, and blue solid lines correspond to the results between 16 and 8 m, 8 and 2 m, and 16 and 2 m, respectively. Color dash lines represent Ogive functions corresponding to the color solid lines. Two vertical dash lines indicate the frequency range of large eddies (i.e., 0.013–0.1 Hz).

dynamic (thermal) attributes of large eddies when these eddies penetrate downward across layers thereby contributing unevenly to fluxes and thus causing flux gradients.

To test this hypothesis, we first examine the effect of large eddies on flux gradients and at what frequencies flux gradients are sustained. Specifically, the scale dependence of cross-layer differences in momentum and kinematic heat fluxes is evaluated using the cross-layer differences in the cospectra of momentum and kinematic heat fluxes calculated as follows:

$$\Delta CO_{uw}(f) = \left| \frac{CO_{uw_{upper}}(f) - CO_{uw_{lower}(f)}}{CO_{uw_{lower}}(f)} \right|, \tag{5}$$

$$\Delta CO_{w\theta}(f) = \left| \frac{CO_{w\theta_{upper}}(f) - CO_{w\theta_{lower}(f)}}{CO_{w\theta_{lower}}(f)} \right|, \tag{6}$$

where CO_{uw} and $CO_{w\theta}$ are cospectra of momentum and kinematic heat fluxes, respectively, that vary with frequency f (Figure 2). Large cross-layer flux differences occur at the midfrequency range between 0.013 and 0.1 Hz, as indicated by several peaks in the cospectral differences and the largest slope of the corresponding Ogive functions; whereas the cospectral differences are fairly small at the low-frequency range (i.e., $f < 0.013$ Hz) and drop dramatically at the high-frequency range (i.e., $f > 0.1$ Hz). Therefore, we define large eddies as turbulent eddies with scales ranging from 0.013 to 0.1 Hz that contribute significantly to the vertical transport of momentum and heat. In the following analysis, we exclude motions with frequencies smaller than 0.013 Hz to minimize the effects of horizontal advection (i.e., through submeso motions) or horizontal flux divergence.

To examine the influence of large eddies on cross-layer flux divergence or convergence in the coupled SBL, EEMD is employed to extract time series signals of large eddies ($0.1 < f < 0.013$ Hz) for each 5-min run of u',

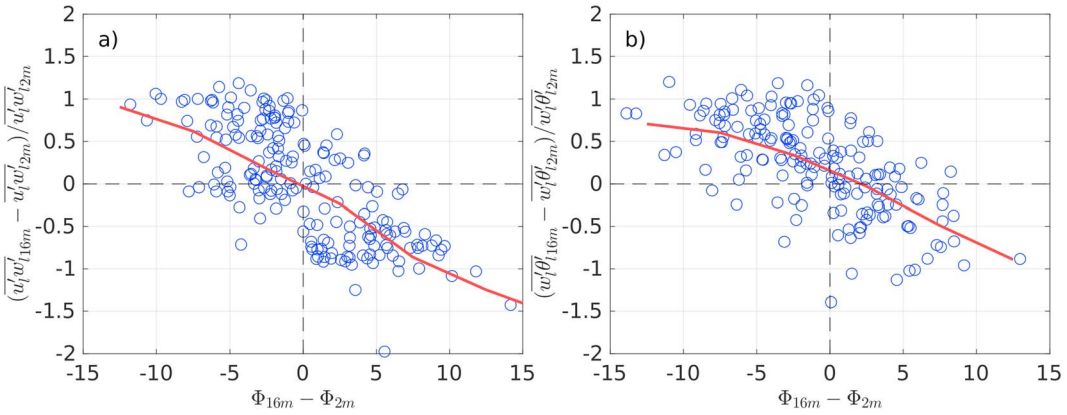

Figure 3. Variations of divergence (or convergence) of momentum flux (a) and kinematic heat flux (b) between 16 and 2 m with cross-layer differences in the phase between vertical velocity (w') and horizontal velocity (u') or potential temperature (θ'). The red fitting curves are calculated with the unweighted bin-averaged method with a bin-width of 1°.

w', and T'. Equation (2) is used to calculate the mean frequency of each IMF. Results indicate that large eddies are represented by the oscillatory components between IMF_2 to IMF_6 ($x_l = \sum_{i=2}^{6} IMF_i$, the subscript l indicates time series signal of large eddies). To ensure that the magnitude of fluctuations associated with large eddies is statistically comparable across layers as expected in the coupled SBL, only the data runs with ΔTKE_l ($\Delta TKE_l = \frac{1}{2}\left(\Delta\sigma_{u_l}{}^2 + \Delta\sigma_{v_l}{}^2 + \Delta\sigma_{w_l}{}^2\right)$, where the subscript l denotes large eddies) being less than 10% are used (i.e., the well coupled SBL based on conventional definitions). As such, the cross-layer flux difference is primarily dependent upon the cross-layer difference in the phase difference between two quantities at the large eddy scales, as shown in Figure 3. Here we only show results between 16 and 2 m, but the other results are alike (Figure S6). As the phase difference between w'_l and u'_l (or θ'_l) in the upper level is larger than that in the lower level, the magnitude of momentum flux ($\overline{w'_l u'_l}$) (or kinematic heat flux, $\overline{w'_l \theta'_l}$) in the upper level is smaller than that in the lower level (i.e., flux divergence), and vice versa (i.e., flux convergence). The fitting curves in Figure 3 indicate that an enlarged cross-layer difference in phase difference leads to the increased flux divergence or convergence (i.e., the increased flux gradients); whereas Figure 1 shows that the increased flux gradients are linked to the enhanced gradients in the corresponding mean variables. These relations suggest that background profiles of mean wind speed and potential temperature, when large in magnitude, alter attributes of the large eddies. The aforementioned alterations are reflected by changes in phase differences as these large eddies penetrate downward, leading to uneven contributions to fluxes across layers and thus flux gradients. The underlying physical processes are explained below.

In the coupled SBL with strong winds, large eddies generated aloft with scales commensurate with the measurement height effectively sweep and impinge the surface, transporting the warm air aloft downward (i.e., $w'_l < 0$, $u'_l > 0$, and $\theta'_l > 0$) and thus leading to negative momentum and kinematic heat fluxes ($\overline{u'_l w'_l} < 0$ and $\overline{w'_l \theta'_l} < 0$). When the phase difference between w'_l and θ'_l is comparable across layers (i.e., when there is no flux divergence or convergence), different vertical layers are dominated by the same large eddies, and the cross-layer fluctuations of w'_l, u'_l, and θ'_l are almost perfectly correlated, leading to negligible cross-layer differences in variances and fluxes. This is referred to as the "perfectly" coupled SBL (i.e., the no flux divergence case in Figure S7 and Table S2). As large eddies penetrate downward indicated by negative time lags in turbulence time series between layers (Table S3), vertical velocity fluctuations (i.e., w'_l) at a lower level can still be the same as those at the higher level in the SBL typically with small background vertical velocity. The smaller lag in w'_l across layers compared to u'_l and θ'_l may be due to the pressure perturbations being coherent vertically. On the other hand, when the background profiles of mean wind speed and potential temperature vary strongly across layers, this leads to different background wind and potential temperature to which the attributes of large eddies are referenced and thus different u'_l and θ'_l as large eddies penetrate across layers. As a consequence, such different u'_l and θ'_l yield flux divergence or convergence between these two levels (i.e., the flux divergence case in Figure S7 and Table S2).

Further analysis shows that the cross-layer difference of the u' and θ' spectra at low-frequency range increases with the enlarged cross-layer phase difference, while the cross-layer difference of w' spectra energy is insensitive to the cross-layer phase difference (Figure S8). It confirms that under the influence of downward penetrating large eddies, the distorted background profiles of mean wind speed and potential temperature can lead to distinct fluctuation patterns in u' and θ' between layers and thus flux divergence or convergence. This reasoning is supported by a scaling argument provided in the next section.

3.3. Scaling Arguments

For stationary and planar-homogeneous atmospheric surface layer (ASL) flows, budget equations for momentum and kinematic heat fluxes can be expressed as (Stull, 1988)

$$\frac{\partial \overline{u'w'}}{\partial t} = 0 = -\overline{w'^2}\frac{\partial \overline{u}}{\partial z} - \frac{\partial \overline{w'u'w'}}{\partial z} - \frac{1}{\rho}\frac{\partial \overline{u'P'}}{\partial z} + \frac{g}{\overline{\theta}}\overline{u'\theta'}, \tag{7}$$

$$\frac{\partial \overline{w'\theta'}}{\partial t} = 0 = -\overline{w'^2}\frac{\partial \overline{\theta}}{\partial z} - \frac{\partial \overline{w'\theta'w'}}{\partial z} - \frac{1}{\rho}\frac{\partial \overline{\theta'P'}}{\partial z} + \frac{g}{\overline{\theta}}\overline{\theta'\theta'}. \tag{8}$$

The terms on the right-hand side (RHS) of equations (7) or (8) include the production term associated with the mean profile of horizontal velocity (or potential temperature), the third-order turbulent transport of momentum flux (or kinematic heat flux), the pressure decorrelation term due to the interaction between pressure and velocity (or temperature), and the buoyancy term associated with thermal stratification. Note that the molecular destruction term is ignored as its magnitude is much smaller than the other terms (Katul et al., 2013, 2014; Li et al., 2018). The Rotta (1951) model retaining the linear component is then employed to parameterize the pressure decorrelation terms

$$-\frac{1}{\rho}\frac{\partial \overline{u'P'}}{\partial z} = -C\frac{\overline{u'w'}}{\tau_u}, \tag{9}$$

$$-\frac{1}{\rho}\frac{\partial \overline{\theta'P'}}{\partial z} = -C\frac{\overline{w'\theta'}}{\tau_\theta}, \tag{10}$$

where C is a proportionality coefficient, τ_u and τ_θ are the relaxation time scales delineating how fast a turbulent eddy loses its coherency (Li, 2019; Li et al., 2018). To simplify the calculation, C, τ_u, and τ_θ are considered as constants. Substituting equations (9) and (10) into equations (7) and (8), respectively, and then taking the derivative with respect to z yield

$$\frac{\partial \overline{u'w'}}{\partial z} = \frac{\tau_u}{C}\left[\frac{\partial}{\partial z}\left(-\overline{w'^2}\frac{\partial \overline{u}}{\partial z}\right) + \frac{\partial}{\partial z}\left(-\frac{\partial \overline{w'u'w'}}{\partial z}\right) + \frac{\partial}{\partial z}\left(\frac{g}{\overline{\theta}}\overline{u'\theta'}\right)\right], \tag{11}$$

$$\frac{\partial \overline{w'\theta'}}{\partial z} = \frac{\tau_\theta}{C}\left[\frac{\partial}{\partial z}\left(-\overline{w'^2}\frac{\partial \overline{\theta}}{\partial z}\right) + \frac{\partial}{\partial z}\left(-\frac{\partial \overline{w'\theta'w'}}{\partial z}\right) + \frac{\partial}{\partial z}\left(\frac{g}{\overline{\theta}}\overline{\theta'\theta'}\right)\right]. \tag{12}$$

These two equations indicate that the gradients in turbulence production (i.e., $\frac{\partial}{\partial z}\left(-\overline{w'^2}\frac{\partial \overline{u}}{\partial z}\right)$ and $\frac{\partial}{\partial z}\left(-\overline{w'^2}\frac{\partial \overline{\theta}}{\partial z}\right)$), turbulent flux transport (i.e., $\frac{\partial}{\partial z}\left(-\frac{\partial \overline{w'u'w'}}{\partial z}\right)$ and $\frac{\partial}{\partial z}\left(-\frac{\partial \overline{w'\theta'w'}}{\partial z}\right)$), and buoyancy destruction (i.e., $\frac{\partial}{\partial z}\left(\frac{g}{\overline{\theta}}\overline{u'\theta'}\right)$ and $\frac{\partial}{\partial z}\left(\frac{g}{\overline{\theta}}\overline{\theta'\theta'}\right)$) contribute to flux gradients. Here each of the turbulence production and turbulent flux transport terms is first calculated in two bulk layers between 16 and 8 m and between 8 and 2 m. These two values for each term in the two bulk layers are then used to calculate the gradient

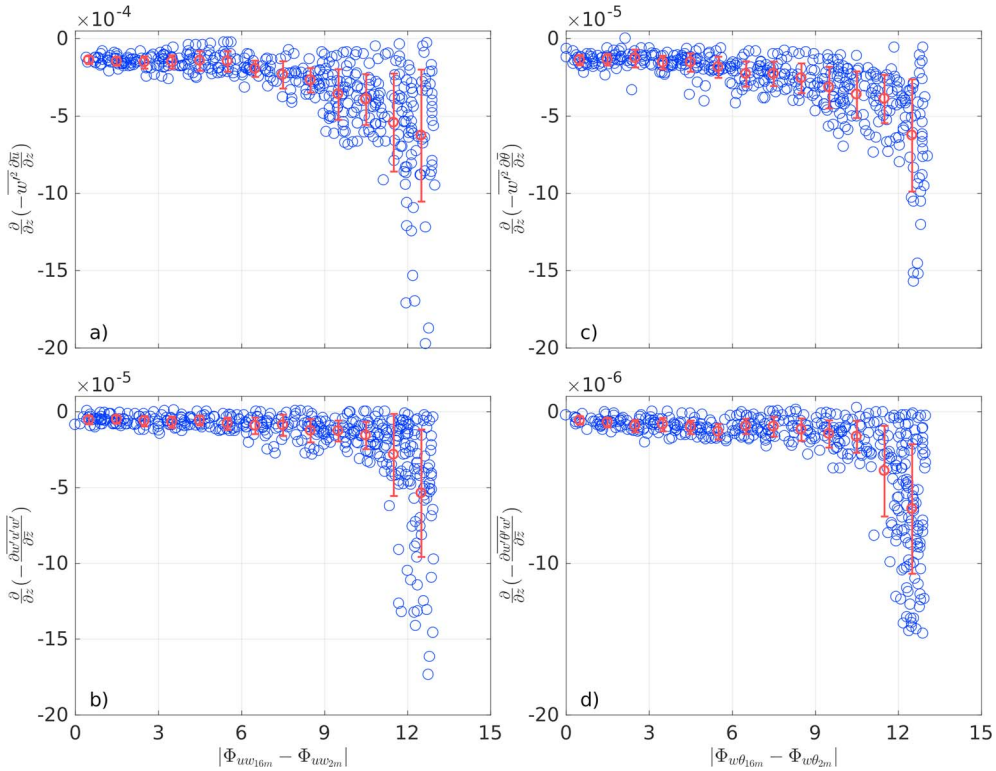

Figure 4. Variations of gradients in the turbulent production terms (a and b) and flux transport terms (c and d) with the cross-layer differences in the phase between vertical velocity (w') and horizontal velocity (u') or potential temperature (θ'). Left (a and b) and right panels (c and d) show the terms associated with momentum and kinematic heat fluxes, respectively. The red circles and error bars refer to the bin averages and corresponding standard deviations, respectively. To emphasize the influence of large eddies on cross-layer transport, the time series associated with large eddies are used for calculating the gradients of the flux transport term (i.e., $\frac{\partial}{\partial z}\left(-\frac{\partial \overline{w'u'w'}}{\partial z}\right)$ and $\frac{\partial}{\partial z}\left(-\frac{\partial \overline{w'\theta'w'}}{\partial z}\right)$ in equations (11) and (12), respectively), while the original time series are used for calculating the turbulence production term (i.e., $\frac{\partial}{\partial z}\left(-\overline{w'^2}\frac{\partial \overline{u}}{\partial z}\right)$ and $\frac{\partial}{\partial z}\left(-\overline{w'^2}\frac{\partial \overline{\theta}}{\partial z}\right)$ equations (11) and (12), respectively).

for each term as shown in Figure 4. However, note that the turbulence production and turbulent flux transport terms shown in Figure 5 are calculated between 16 and 2 m for consistency with the prior analysis.

Since the gradients of the buoyancy term are small (Figures S4 and S5 and Table S1), the flux gradients are primarily attributed to the cross-layer difference in the turbulent production and the turbulent flux transport as quantified by the first and second terms of the RHS of equations (11) and (12), respectively. Under the circumstance that the first and second terms of the RHS of equations (11) and (12) approach zero (i.e., no cross-layer differences for these two terms), no flux gradient occurs. As analyzed in the previous section, the ASL without flux gradient is under the influence of large eddies with small cross-layer differences in phase differences between w'_l and u'_l (or θ'_l). These statements are clearly supported by Figure 4, which shows that under the conditions with small cross-layer differences in phase difference ($|\phi_{16m} - \phi_{2m}|$), the gradients in both the turbulence production terms ($\frac{\partial}{\partial z}\left(-\overline{w'^2}\frac{\partial \overline{u}}{\partial z}\right)$ and $\frac{\partial}{\partial z}\left(-\overline{w'^2}\frac{\partial \overline{\theta}}{\partial z}\right)$ in equations (11) and (12), respectively) and the turbulent flux transport term ($\frac{\partial}{\partial z}\left(-\frac{\partial \overline{w'u'w'}}{\partial z}\right)$ and $\frac{\partial}{\partial z}\left(-\frac{\partial \overline{w'\theta'w'}}{\partial z}\right)$ in equations (11) and (12), respectively) are negligibly small. Figure 5 further shows that this condition is linked to a coupled

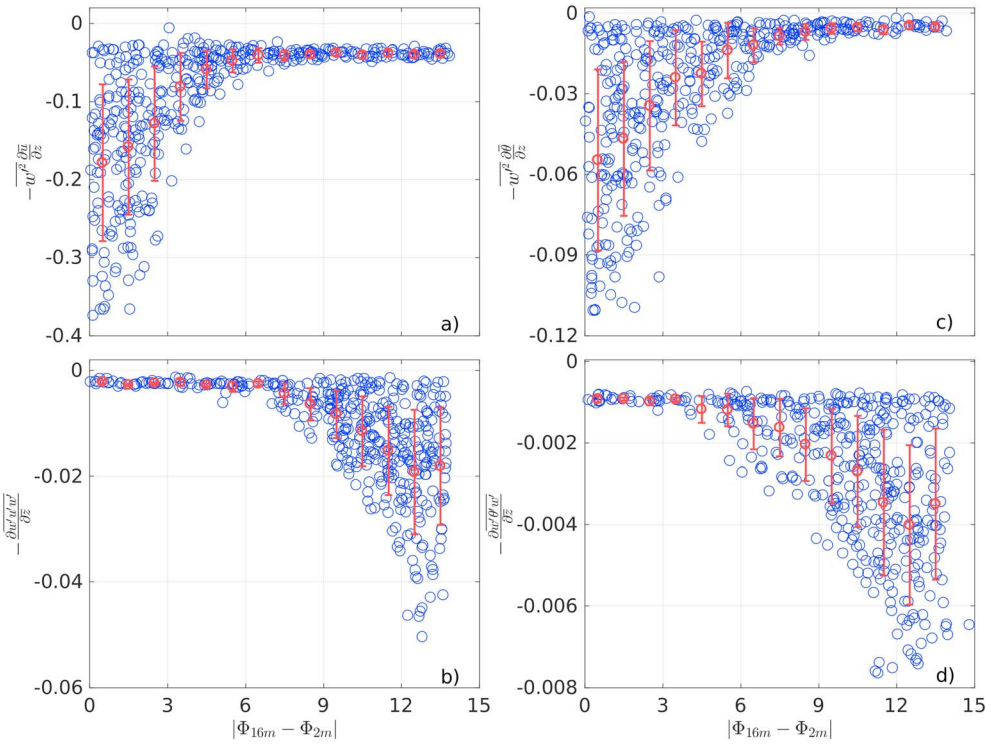

Figure 5. Variations of the turbulent production term (a and c) and flux transport term (b and d) with the cross-layer differences in phase between vertical velocity (w') and horizontal velocity (u') or potential temperature (θ'). Left (a and b) and right (c and d) panels show the terms associated with momentum and kinematic heat fluxes, respectively. The red circles and error bars refer to the bin averages and corresponding standard deviations, respectively. To emphasize the influence of large eddies on cross-layer transport, the time series associated with large eddies are used for calculating third-order terms in equations (7) and (8) (i.e., $\frac{\partial w_l' u_l' w_l'}{\partial z}$ and $\frac{\partial \overline{w_l' \theta_l' w_l'}}{\partial z}$), while the original time series are used for calculating the turbulence production term.

SBL where the turbulence production is large (i.e., $-\overline{w'^2}\frac{\partial \overline{u}}{\partial z}$ and $-\overline{w'^2}\frac{\partial \overline{\theta}}{\partial z}$ in equations (7) and (8), respectively) and the turbulent flux transport between layers is comparable (i.e., $-\frac{\partial \overline{w'u'w'}}{\partial z}$ and $-\frac{\partial \overline{w'\theta'w'}}{\partial z}$ in equations (7) and (8) tend to be zero). Results between 16 and 8 m and those between 8 and 2 m are alike and shown in Figure S9. These results suggest that sufficiently strong turbulence production term results in a well coupled SBL that is strongly modulated by large eddies with vertically synchronized phases thereby leading to a small flux gradient.

Conversely, an increase or a decrease in the first and second terms of the RHS of equations (11) and (12) (i.e., an increase or a decrease in the cross-layer differences for these two terms) would yield an increased flux gradient. It has been found in the last section that these increased flux gradients are caused by large eddies with increased cross-layer differences in the phase difference between w'_l and θ'_l (or u'_l). This relation is also supported by Figure 4, which shows that the increased cross-layer differences in the phase difference ($|\phi_{16m} - \phi_{2m}|$) correspond to the increased gradients in both the turbulence production and turbulent flux transport terms. This condition occurs in a coupled SBL where the turbulence production is weak and the gradient of turbulent flux transport is large (Figures 5 and S9). The weak turbulence production tends to occur in a relatively more stratified SBL with weak shear and distorted mean profiles. As such, different vertical layers are dominated by large eddies with distinct attributes in θ'_l and u'_l thereby contributing unevenly to fluxes.

As a bridge between this analysis and the utility of MOST in the SBL, equations (7) and (8) closed using equations (9) and (10) in the absence of the gravitational terms are rearranged and lead to

$$\overline{u'w'} = \frac{\tau_u}{C}\left(-\overline{w'^2}\frac{\partial\overline{u}}{\partial z} - \frac{\partial\overline{w'u'w'}}{\partial z}\right), \tag{13}$$

$$\overline{w'\theta'} = \frac{\tau_\theta}{C}\left(-\overline{w'^2}\frac{\partial\overline{\theta}}{\partial z} - \frac{\partial\overline{w'\theta'w'}}{\partial z}\right). \tag{14}$$

Clearly, the failure of flux-gradient relations or MOST schemes is linked here to the large turbulent flux transport terms. Hence, the ratios $R_{LLu} = -\frac{\partial\overline{w'u'w'}}{\partial z}/\left(-\overline{w'^2}\frac{\partial\overline{u}}{\partial z}\right)$ and $R_{LLT} = -\frac{\partial\overline{w'\theta'w'}}{\partial z}/\left(-\overline{w'^2}\frac{\partial\overline{\theta}}{\partial z}\right)$ for large eddies only have been computed and have been shown to increase with increasing magnitudes of $\frac{\partial\overline{u}}{\partial z}$ and $\frac{\partial\overline{\theta}}{\partial z}$ (Figure S10). A naïve expectation is that when the magnitudes of $\frac{\partial\overline{u}}{\partial z}$ and $\frac{\partial\overline{\theta}}{\partial z}$ increase, the production terms $\left(-\overline{w'^2}\frac{\partial\overline{u}}{\partial z}\right)$ and $\left(-\overline{w'^2}\frac{\partial\overline{\theta}}{\partial z}\right)$ proportionally increase resulting in a decrease in the ratios of the flux transport to production terms. However, the analysis here suggests that a small $\overline{w'^2}$ (suppressed by thermal stratification in the SBL) and the generation of flux transport terms associated with large eddies acting on the large mean gradients lead to ratios R_{LLu} and R_{LLT} exceeding unity (Figure S10). These large R_{LLu} and R_{LLT} are, of course, the main reason why flux-gradient theory (or MOST) fails as discussed elsewhere (Li et al., 2018). The large magnitudes of in $\frac{\partial\overline{u}}{\partial z}$ and $\frac{\partial\overline{\theta}}{\partial z}$ are, to large degree, anchored by boundary conditions at the surface (friction velocity and radiative cooling) as well as the SBL aloft. Transport between layers in the SBL is primarily determined by the efficiency of large eddies to bring heat and momentum between surface and the state of the SBL aloft. Large magnitudes of $\frac{\partial\overline{u}}{\partial z}$ and $\frac{\partial\overline{\theta}}{\partial z}$ distort the phase relations across layers for u'_l and θ'_l but not for w'_l, leading to large flux gradients.

4. Conclusions

Using data collected by multilevel EC systems positioned on a 62-m meteorological tower over a large open flat terrain, mechanisms for sustaining vertical gradients of momentum and kinematic heat fluxes in the coupled SBL with strong near-surface shear and well mixed TKE are analyzed. Cross-layer cospectra indicate that large turbulent eddies with scales from 0.013–0.1 Hz contribute significantly to flux gradients. In a well coupled SBL with strong turbulence production, no flux gradients are evident. The argument put forth here is that large eddies contribute evenly to vertical gradients in the turbulent flux transport and production terms across layers. Such large eddies are linked to minimal cross-layer alteration in phase differences between vertical velocity and potential temperature (or horizontal wind). In a slightly layered SBL with weak turbulence production, eddies crossing disjointed layers experience distortions to their phase angle and thus contribute unevenly to fluxes. This finding is also supported by the different magnitudes of the turbulent flux transport terms across layers.

Acknowledgments
We wish to acknowledge S. Beard, T. Strong, and B. Reese from the Field Research Division of NOAA as well as E. Russell and Z. Gao for their assistance during the field campaign. We thank two anonymous reviewers for their constructive comments to improve the quality of this manuscript. H. L. acknowledges support by National Science Foundation (NSF-AGS-1419614). C. L. acknowledges support by China Scholarship Council (CSC) and National Science Foundation (NSF-AGS-1419614). G. K. also acknowledges support from NSF (NSF-EAR-1344703, NSF-AGS-1644382, and NSF-DGE-1068871) and from the Department of Energy (DE-SC-0011461). According to the AGU publications Data Policy, the data used in this paper are deposited in a public repository (http://micromet.paccar.wsu.edu/paperdata/Lan_GRL.zip).

References

Acevedo, O. C., Costa, F. D., & Degrazia, G. A. (2012). The coupling state of an idealized stable boundary layer. *Boundary-Layer Meteorology*, *145*(1), 211–228. https://doi.org/10.1007/s10546-011-9676-3

Acevedo, O. C., Mahrt, L., Puhales, F. S., Costa, F. D., Medeiros, L. E., & Degrazia, G. A. (2016). Contrasting structures between the decoupled and coupled states of the stable boundary layer. *Quarterly Journal of the Royal Meteorological Society*, *142*(695), 693–702. https://doi.org/10.1002/qj.2693

Dyer, A. J., & Hicks, B. B. (1970). Flux-gradient relationships in the constant flux layer. *Quarterly Journal of the Royal Meteorological Society*, *96*(410), 715–721. https://doi.org/10.1002/qj.49709641012

Finn, D., Clawson, K. L., Eckman, R. M., Carter, R. G., Rich, J. D., Strong, T. W., et al. (2015). Project Sagebrush Phase 1, NOAA Technical Memorandum OAR ARL-268, Air Resources Laboratory, Idaho Falls, Idaho (338 pp.). https://doi.org/10.7289/V5VX0DHV

Finn, D., Reese, B., Butler, B., Wagenbrenner, N., Clawson, K. L., Rich, J., et al. (2016). Evidence for gap flows in the Birch Creek Valley, Idaho. *Journal of the Atmospheric Sciences*, *73*(12), 4873–4894. https://doi.org/10.1175/JAS-D-16-0052.1

Foken, T., Göockede, M., Mauder, M., Mahrt, L., Amiro, B., & Munger, W. (2005). Post-field data quality control. In X. Lee, W. Massman, & B. Law (Eds.), *Handbook of Micrometeorology: A Guide for Surface Flux Measurement and Analysis*, (pp. 181–208). Dordrecht, Netherlands: Springer. https://doi.org/10.1007/1-4020-2265-4_9

Gao, Z., Liu, H., Katul, G. G., & Foken, T. (2017). Non-closure of the surface energy balance explained by phase difference between vertical velocity and scalars of large atmospheric eddies. *Environmental Research Letters*, *12*(3), 34025. https://doi.org/10.1088/1748-9326/aa625b

Gao, Z., Liu, H., Russell, E. S., Huang, J., Foken, T., & Oncley, S. P. (2016). Large eddies modulating flux convergence and divergence in a disturbed unstable atmospheric surface layer. *Journal of Geophysical Research: Atmospheres*, *121*, 1475–1492. https://doi.org/10.1002/2015JD024529

Huang, N. E., Shen, Z., Long, S. R., Wu, M. C., Shih, H. H., Zheng, Q., et al. (1998). The empirical mode decomposition and the Hilbert spectrum for nonlinear and non-stationary time series analysis. *Proceedings of the Royal Society A*, *454*(1971), 903–995. https://doi.org/10.1098/rspa.1998.0193

Huang, N. E., & Wu, Z. (2008). A review on Hilbert-Huang transform: Method and its applications to geophysical studies. *Reviews of Geophysics*, *46*, RG2006. https://doi.org/10.1029/2007RG000228

Jensen, D. D., Nadeau, D. F., Hoch, S. W., & Pardyjak, E. R. (2016). Observations of near-surface heat-flux and temperature profiles through the early evening transition over contrasting surfaces. *Boundary-Layer Meteorology*, *159*(3), 567–587. https://doi.org/10.1007/s10546-015-0067-z

Kaimal, J. C., & Finnigan, J. J. (1994). *Atmospheric boundary layer flows: Their structure and measurement*. New York: Oxford University Press.

Katul, G., Porporato, A., Manes, C., & Meneveau, C. (2013). Co-spectrum and mean velocity in turbulent boundary layers. *Physics of Fluids*, *25*(9), 091702. https://doi.org/10.1063/1.4821997

Katul, G. G., Porporato, A., Shah, S., & Bou-Zeid, E. (2014). Two phenomenological constants explain similarity laws in stably stratified turbulence. *Physical Review E*, *89*(2), 023007. https://doi.org/10.1103/PhysRevE.89.023007

Lan, C., Liu, H., Li, D., Katul, G. G., & Finn, D. (2018). Distinct turbulence structures in stably stratified boundary layers with weak and strong surface shear. *Journal of Geophysical Research: Atmospheres*, *123*(15), 7839–7854. https://doi.org/10.1029/2018JD028628

Li, D. (2019). Turbulent Prandtl number in the atmospheric boundary layer—Where are we now? *Atmospheric Research.*, *216*, 86–105. https://doi.org/10.1016/j.atmosres.2018.09.015

Li, D., & Bou-Zeid, E. (2011). Coherent structures and the dissimilarity of turbulent transport of momentum and scalars in the unstable atmospheric surface layer. *Boundary-Layer Meteorology*, *140*(2), 243–262. https://doi.org/10.1007/s10546-011-9613-5

Li, D., Katul, G. G., & Liu, H. (2018). Intrinsic constraints on asymmetric turbulent transport of scalars within the constant flux layer of the lower atmosphere. *Geophysical Research Letters*, *45*(4), 2022–2030. https://doi.org/10.1002/2018GL077021

Liang, J., Zhang, L., Wang, Y., Cao, X., Zhang, Q., Wang, H., & Zhang, B. (2014). Turbulence regimes and the validity of similarity theory in the stable boundary layer over complex terrain of the Loess Plateau, China. *Journal of Geophysical Research: Atmospheres*, *119*, 6009–6021. https://doi.org/10.1002/2014JD021510

Liu, H., Peters, G., & Foken, T. (2001). New equations for sonic temperature variance and buoyancy heat flux with an omnidirectional sonic anemometer. *Boundary-Layer Meteorology*, *100*(3), 459–468. https://doi.org/10.1023/A:1019207031397

Liu, H., Zhang, Q., Katul, G. G., Cole, J. J., Chapin, F. S. III, & MacIntyre, S. (2016). Large CO_2 effluxes at night and during synoptic weather events significantly contribute to CO_2 emissions from a reservoir. *Environmental Research Letters*, *11*(6), 64001. https://doi.org/10.1088/1748-9326/11/6/064001

Mahrt, L. (2014). Stably stratified atmospheric boundary layers. *Annual Review of Fluid Mechanics*, *46*(1), 23–45. https://doi.org/10.1146/annurev-fluid-010313-141354

Mahrt, L., Thomas, C. K., Grachev, A. A., & Persson, P. O. G. (2018). Near-surface vertical flux divergence in the stable boundary layer. *Boundary-Layer Meteorology*, *169*(3), 373–393. https://doi.org/10.1007/s10546-018-0379-x

Monahan, A. H., Rees, T., He, Y., & McFarlane, N. (2015). Multiple regimes of wind, stratification, and turbulence in the stable boundary layer. *Journal of the Atmospheric Sciences*, *72*(8), 3178–3198. https://doi.org/10.1175/JAS-D-14-0311.1

Monin, A. S., & Obukhov, A. M. (1954). Basic laws of turbulent mixing in the surface layer of the atmosphere. *Tr. Akad. Nauk SSSR Geophiz. Inst.*, *24*(151), 163–187.

Mortarini, L., Cava, D., Giostra, U., Acevedo, O., Nogueira Martins, L. G., Soares de Oliveira, P. E., & Anfossi, D. (2018). Observations of submeso motions and intermittent turbulent mixing across a low level jet with a 132-m tower. *Quarterly Journal of the Royal Meteorological Society*, *144*(710), 172–183. https://doi.org/10.1002/qj.3192

Rotta, J. (1951). Statistical theory of nonhomogeneous turbulence. *Zeitschrift für Physik*, *131*(1), 51–77. https://doi.org/10.1007/BF01329645

Schotanus, P., Nieuwstadt, F. T. M., & De Bruin, H. A. R. (1983). Temperature measurement with a sonic anemometer and its application to heat and moisture fluxes. *Boundary-Layer Meteorology*, *26*(1), 81–93. https://doi.org/10.1007/BF00164332

Sorbjan, Z., & Czerwinska, A. (2013). Statistics of turbulence in the stable boundary layer affected by gravity waves. *Boundary-Layer Meteorology*, *148*(1), 73–91. https://doi.org/10.1007/s10546-013-9809-y

Stull, R. (1988). *An introduction to boundary layer meteorology*. Dordrecht: Kluwer Academic Publishers. https://doi.org/10.1007/978-94-009-3027-8

Sun, J., Lenschow, D. H., LeMone, M. A., & Mahrt, L. (2016). The role of large-coherent-eddy transport in the atmospheric surface layer based on CASES-99 observations. *Boundary-Layer Meteorology*, *160*(1), 83–111. https://doi.org/10.1007/s10546-016-0134-0

Sun, J., Mahrt, L., Banta, R. M., & Pichugina, Y. L. (2012). Turbulence regimes and turbulence intermittency in the stable boundary layer during CASES-99. *Journal of the Atmospheric Sciences*, *69*(1), 338–351. https://doi.org/10.1175/JAS-D-11-082.1

Webb, E. K., Pearman, G. I., & Leuning, R. (1980). Correction of flux measurements for density effects due to heat and water vapour transfer. *Quarterly Journal of the Royal Meteorological Society*, *106*(447), 85–100. https://doi.org/10.1002/qj.49710644707

Wei, W., Zhang, H. S., Schmitt, F. G., Huang, Y. X., Cai, X. H., Song, Y., & Zhang, H. (2017). Investigation of turbulence behaviour in the stable boundary layer using arbitrary-order Hilbert spectra. *Boundary-Layer Meteorology*, *163*(2), 311–326. https://doi.org/10.1007/s10546-016-0227-9